Pergamon

Int. J. Solids Structures Vol. 35, Nos 31–32, pp. 4257–4274, 1998

0020–7683/98 $19.00 + .00

PII: S0020–7683(97)00313–2

DISCONTINUOUS FAILURE ANALYSIS FOR MODE-I AND MODE-II LOCALIZATION PROBLEMS

L. J. SLUYS* and A. H. BERENDS
Delft University of Technology, Department of Civil Engineering, P.O. Box 5048, 2600 GA Delft, The Netherlands

(*Received* 20 *November* 1996; *in revised form* 21 *April* 1997)

Abstract—In this paper failure is assumed to be a discrete phenomenon. A modelling in which a crack or a shear band is incorporated in the shape functions of the finite element formulation is used. A discontinuous function of the displacement gradients acts as an additional localized mode with a length scale parameter that is independent of the element size. A predefinition of the failure zone is not necessary and the crack or shear band can be described with a relatively small number of finite elements. The model is elaborated for simple mode-I and mode-II problems. A comparison with standard continuum models for failure has been made. © 1998 Elsevier Science Ltd. All rights reserved.

1. INTRODUCTION

For the description of failure processes in brittle and ductile materials roughly two approaches can be distinguished: the continuum modelling vs the discrete modelling. In continuum models the failure process is assumed to be smeared over the finite element. As a consequence standard continuum models for mode-I and mode-II failure behavior that describe softening behavior result in mesh-dependent solutions. Due to the lack of an internal length scale the size of the failure process zone is left unspecified. In finite element calculations the length scale is therefore set by the size of the finite element. As a remedy for this behavior several techniques have been proposed such as nonlocal models, gradient models, rate-dependent models and micro-polar models for mode-II localization problems (Aifantis, 1984; Pijaudier-Cabot and Bažant, 1987; Needleman, 1988; Lasry and Belytschko, 1988; Mühlhaus and Aifantis, 1991; de Borst *et al.*, 1992; Sluys, 1992; Sluys *et al.*, 1992). All models (i) introduce a length scale parameter (ii) keep the mathematical problem well-posed and (iii) remove mesh-size and mesh-orientation dependence. Their major disadvantage is that the localization zone must be analyzed with a very fine mesh. Since the strain profile in the localization zone is continuous with steep gradients a large number of elements is needed to describe this accurately. The exact number of elements that is needed is determined by the length scale parameter (size of the localization zone), the constitutive equation for softening (shape of the localization zone) and the type of element (order of interpolation) that is used. Remeshing strategies are necessary to make these models applicable for large scale computations.

An alternative approach is the modelling of the failure zone as a discrete phenomenon. For instance interface elements can be used to model failure in a discontinuous manner. The crack or shear band is modelled by discontinuous displacements along the interface elements. A disadvantage is that the localization zone should be predefined which is a problem in cases where the location of the failure zone is unknown. The use of a mesh-realignment procedure can overcome this problem but this technique is difficult to implement (Larsson, 1990). A predefinition of the failure zone is not necessary when the discontinuity that represents the crack or the shear band is already incorporated in the shape functions of the finite element. Two models have been discussed in literature in which the addition of so-called localized modes to the element formulation is used for the modelling of failure processes. Firstly, a modelling with strong discontinuities is proposed

* Author to whom correspondence should be addressed.

by e.g. Ortiz *et al.* (1987), Klisinski *et al.* (1991), Simo *et al.* (1993), Simo and Oliver (1994), Armero and Garikipati (1995), Larsson *et al.* (1995), Lotfi and Shing (1995) and Larsson and Runesson (1996), in which a jump in the displacement field is assumed. To overcome the problem of infinite strains and Dirac-delta functions in the constitutive description the concept of a regularized softening parameter is used which is made dependent on a length scale parameter. This parameter plays the role of characteristic length in the model. Secondly, Belytschko *et al.* (1988) used a model with the discontinuity formulated in the displacement gradient field or strain field. This is a so-called weak discontinuity model. A length scale parameter defines the size of the localization zone in which the additional jump functions are active. This length scale parameter plays a similar role as in the above mentioned continuum models. It is independent of the finite element size and the determination of it should be carried out by a combined experimental/numerical study. In this paper the second approach will be followed for the modelling of mode-I failure with a crack model and mode-II failure with a plasticity model. The features of the approach will be discussed by means of simple one- and two-dimensional finite element calculations. A mesh-sensitivity study has been carried out and the model is compared to standard models for failure. Two-dimensional simulations with the weak discontinuity model have been used to assess the propagation of localization bands in structured and unstructured meshes.

2. KINEMATICS OF DISCONTINUOUS FAILURE

In the approach proposed in this paper a discontinuity of velocity gradient at the edges of the localization zone is assumed (see Fig. 1). The displacements and the velocities in the localized area are still continuous. For a jump in velocity gradient $\dot{u}_{i,j}$ between cracked and non-cracked material or between the area inside and outside a shear band we define

$$\left[\!\left[\dot{u}_{i,j}\right]\!\right] = \bar{\alpha} m_i n_j, \tag{1}$$

in which the vector $\mathbf{n}$ is the normal to the discontinuity plane, the vector $\mathbf{m}$ defines the nature of the discontinuity and $\bar{\alpha}$ is the jump coefficient. For a pure mode-I failure plane $\mathbf{m}$ is aligned with $\mathbf{n}$ and $\mathbf{n}^{\mathrm{T}}\mathbf{m} = 1$, on the other hand for a pure mode-II failure $\mathbf{m}$ is perpendicular to $\mathbf{n}$ and $\mathbf{n}^{\mathrm{T}}\mathbf{m} = 0$. Furthermore in Fig. 1 the angle θ determines the orientation of the discontinuity plane and the parameter l plays the role of the localization band width. This parameter appears as an independent material parameter and is not set by the finite element size. From the jump of velocity gradient we can define the jump in strain rate according to

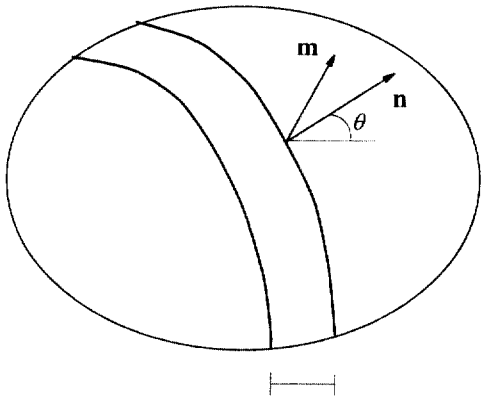

Fig. 1. Definition of the displacement gradient discontinuity.

$$[\![\dot{\varepsilon}_{ij}]\!] = \frac{\bar{\alpha}}{2}(m_i n_j + m_j n_i) \tag{2}$$

or for the plane stress situation

$$\begin{pmatrix} [\![\dot{\varepsilon}_{xx}]\!] \\ [\![\dot{\varepsilon}_{yy}]\!] \\ [\![\dot{\gamma}_{xy}]\!] \end{pmatrix} = \bar{\alpha} \begin{pmatrix} m_x \cos\theta \\ m_y \sin\theta \\ m_x \sin\theta + m_y \cos\theta \end{pmatrix} = \bar{\alpha}\mathbf{q}, \tag{3}$$

in which $(n_x, n_y)^{\mathrm{T}} = (\cos\theta, \sin\theta)^{\mathrm{T}}$. At both edges of the localization band we distinguish jumps in the displacement gradient. We define two jump coefficients $\bar{\alpha}_1$ and $\bar{\alpha}_2$ that determine the additional strain field of the localized mode. The jump $\bar{\alpha}_1$ represents the decrease in strain in the elastic area and $\bar{\alpha}_2$ denotes the increase of strain in the inelastic area, both with respect to a formulation without additional jump functions. We can now derive expressions for the strain rate outside the band $\dot{\boldsymbol{\varepsilon}}_1$ and inside the band $\dot{\boldsymbol{\varepsilon}}_2$ according to

$$\dot{\boldsymbol{\varepsilon}}_1 = \mathbf{L}\dot{\mathbf{u}} - \bar{\alpha}_1\mathbf{q} \tag{4}$$

$$\dot{\boldsymbol{\varepsilon}}_2 = \mathbf{L}\dot{\mathbf{u}} + \bar{\alpha}_2\mathbf{q}, \tag{5}$$

in which the differential operator matrix $\mathbf{L}$ for plane stress is defined as

$$\mathbf{L} = \begin{bmatrix} \dfrac{\partial \cdot}{\partial x} & 0 \\ 0 & \dfrac{\partial \cdot}{\partial y} \\ \dfrac{\partial \cdot}{\partial y} & \dfrac{\partial \cdot}{\partial x} \end{bmatrix}. \tag{6}$$

In a finite element set-up we discretize the continuous displacement field $\mathbf{u}$ by

$$\dot{\mathbf{u}} = \mathbf{H}\dot{\mathbf{a}}, \tag{7}$$

in which the matrix $\mathbf{H}$ contains the interpolation polynomials and $\dot{\mathbf{a}}$ are the nodal velocities. If we substitute eqn (7) and introduce the strain-nodal displacement matrix $\mathbf{B} = \mathbf{LH}$ eqns (4) and (5) become

$$\dot{\boldsymbol{\varepsilon}}_1 = \mathbf{B}\dot{\mathbf{a}} - \bar{\alpha}_1\mathbf{q} \tag{8}$$

$$\dot{\boldsymbol{\varepsilon}}_2 = \mathbf{B}\dot{\mathbf{a}} + \bar{\alpha}_2\mathbf{q}. \tag{9}$$

For convenience we can rewrite eqns (8) and (9) by multiplication of the additional strain field by the scalar quantity $\mathbf{q}^{\mathrm{T}}\mathbf{B}\dot{\mathbf{a}}$ and obtain

$$\dot{\varepsilon}_1 = \bar{\mathbf{B}}_1\dot{\mathbf{a}} \tag{10}$$

and

$$\dot{\varepsilon}_2 = \bar{\mathbf{B}}_2\dot{\mathbf{a}} \tag{11}$$

where

$$\bar{\mathbf{B}}_1 = [\mathbf{I} - \alpha_1 \mathbf{q}\mathbf{q}^T]\mathbf{B} \tag{12}$$

$$\bar{\mathbf{B}}_2 = [\mathbf{I} + \alpha_2 \mathbf{q}\mathbf{q}^T]\mathbf{B} \tag{13}$$

with $\bar{\alpha}_1 = \alpha_1 \mathbf{q}^T \mathbf{B}\dot{\mathbf{a}}$ and $\bar{\alpha}_2 = \alpha_2 \mathbf{q}^T \mathbf{B}\dot{\mathbf{a}}$.

3. MODE-I FAILURE

As discussed above two regions have been defined in a medium that undergoes localization. In the elastic part of the material the total strain rate $\dot{\boldsymbol{\varepsilon}}$ equals the elastic strain rate $\dot{\boldsymbol{\varepsilon}}^e$

$$\dot{\boldsymbol{\varepsilon}}_1 = \dot{\boldsymbol{\varepsilon}}_1^e. \tag{14}$$

and the constitutive equation is given by

$$\dot{\boldsymbol{\sigma}}_1 = \mathbf{D}^e \dot{\boldsymbol{\varepsilon}}_1^e, \tag{15}$$

with matrix $\mathbf{D}^e$ containing the elastic stiffness moduli. For the localized part that represent the cracked material we apply a decomposition of total strain rate $\dot{\boldsymbol{\varepsilon}}$ into the elastic strain rate $\dot{\boldsymbol{\varepsilon}}^e$ and the crack strain rate $\dot{\boldsymbol{\varepsilon}}^{cr}$

$$\dot{\boldsymbol{\varepsilon}}_2 = \dot{\boldsymbol{\varepsilon}}_2^e + \dot{\boldsymbol{\varepsilon}}_2^{cr}. \tag{16}$$

When incorporating the crack stress–crack strain laws it is convenient to use the local n, t-coordinate system in a two-dimensional configuration, which is aligned with the discontinuity (see Fig. 1). This necessitates a transformation between the crack strain rate $\dot{\boldsymbol{\varepsilon}}_2^{cr}$ in the global x, y, z-coordinates and the crack strain rate $\dot{\mathbf{e}}_2^{cr}$ in the local coordinates. The crack strain rate in the local coordinate system is defined as

$$\dot{\mathbf{e}}_2^{cr} = [\dot{e}_2^{nn}, 2\dot{e}_2^{nt}]^T, \tag{17}$$

where $\dot{e}_2^{nn}$ is the mode-I crack normal strain rate and $\dot{e}_2^{nt}$ is the mode-II crack shear strain rate. The relation between local and global strain rates reads

$$\dot{\boldsymbol{\varepsilon}}_2^{cr} = \mathbf{N}\dot{\mathbf{e}}_2^{cr} \tag{18}$$

where $\mathbf{N}$ is the transformation matrix given by

$$\mathbf{N} = \begin{bmatrix} \cos^2\theta & -\sin\theta\cos\theta \\ \sin^2\theta & \sin\theta\cos\theta \\ 2\sin\theta\cos\theta & \cos^2\theta - \sin^2\theta \end{bmatrix}, \tag{19}$$

with θ the inclination angle of the normal of the crack $\mathbf{n}$ with the x-axis (see Fig. 1). The angle is determined by the principal stress direction at the onset of cracking. An essential feature of the model is that $\mathbf{N}$ is fixed upon crack formation so that the concept belongs to the class of fixed crack concepts. If we let the discontinuity plane rotate with principal stresses a so-called rotating discontinuity model can be obtained.

In a similar way we can define a crack stress rate vector

$$\dot{\mathbf{t}}_2 = [\dot{t}_2^{nn}, \dot{t}_2^{nt}]^T. \tag{20}$$

in which $\dot{t}_2^{nn}$ is the mode-I normal crack stress rate and $\dot{t}_2^{nt}$ is the mode-II shear crack stress

rate. The relation between the stress rate in the global coordinate system and the local stress rate can be derived to be

$$\dot{\mathbf{t}}_2 = \mathbf{N}^{\mathrm{T}}\dot{\boldsymbol{\sigma}}_2. \tag{21}$$

To complete the system of equations we need a constitutive model for the elastic contribution of the cracked material given by

$$\dot{\boldsymbol{\sigma}}_2 = \mathbf{D}^{\mathrm{e}}\dot{\boldsymbol{\varepsilon}}_2^{\mathrm{e}}. \tag{22}$$

and the relation between the local crack strain rate and the local crack stress rate

$$\dot{\mathbf{t}}_2 = \mathbf{D}^{\mathrm{cr}}\dot{\mathbf{e}}_2^{\mathrm{cr}} \tag{23}$$

with

$$\mathbf{D}^{\mathrm{cr}} = \begin{bmatrix} h & 0 \\ 0 & \beta\mu \end{bmatrix}, \tag{24}$$

in which h is the mode-I ($h < 0$). The shear stiffness in the crack is obtained by a multiplication of the elastic shear stiffness μ with a shear reduction factor β. Coupling effects between the two modes are not considered. In this model fracture is assumed to be initiated in mode-I and mode-II effects enter upon rotation of the principal stresses.

Now, the overall stress–strain relation of the model with respect to the global coordinate system can be developed. Combining eqns (16) and (22) and subsequent substitution of eqn (18) yields

$$\dot{\boldsymbol{\sigma}}_2 = \mathbf{D}^{\mathrm{e}}[\dot{\boldsymbol{\varepsilon}}_2 - \mathbf{N}\dot{\mathbf{e}}_2^{\mathrm{cr}}]. \tag{25}$$

Premultiplying this equation by $\mathbf{N}^{\mathrm{T}}$ and substituting eqns (21) and (23) yields the relation between the local crack strain rate and the global strain rate

$$\dot{\mathbf{e}}_2^{\mathrm{cr}} = [\mathbf{D}^{\mathrm{cr}} + \mathbf{N}^{\mathrm{T}}\mathbf{D}^{\mathrm{e}}\mathbf{N}]^{-1}\mathbf{N}^{\mathrm{T}}\mathbf{D}^{\mathrm{e}}\dot{\boldsymbol{\varepsilon}}_2. \tag{26}$$

The overall relation between global stress rate and global strain rate is obtained by substituting eqn (26) into (25)

$$\dot{\boldsymbol{\sigma}}_2 = [\mathbf{D}^{\mathrm{e}} - \mathbf{D}^{*}]\dot{\boldsymbol{\varepsilon}}_2 \tag{27}$$

with

$$\mathbf{D}^{*} = \mathbf{D}^{\mathrm{e}}\mathbf{N}[\mathbf{D}^{\mathrm{cr}} + \mathbf{N}^{\mathrm{T}}\mathbf{D}^{\mathrm{e}}\mathbf{N}]^{-1}\mathbf{N}^{\mathrm{T}}\mathbf{D}^{\mathrm{e}}. \tag{28}$$

In this derivation only one crack or discontinuity per integration point is considered, but it is possible that due to the rotation of principal stresses new cracks arise. The crack strain is then decomposed into separate contributions from the multi-directional cracks (Rots, 1988). The integration of eqn (28) can be done by a one-step forward scheme which is exact if the matrices $\mathbf{D}^{\mathrm{e}}$ and $\mathbf{D}^{\mathrm{cr}}$ remain constant during the time step. When, for instance, $\mathbf{D}^{\mathrm{cr}}$ is non-constant a predictor–corrector method can be used in an inner iteration loop to determine the incremental stresses. Secant unloading is used which implies that also in the unloading stage a split up of the finite element into an elastic part Ω_1 and a localized part Ω_2 is applied.

In the model the unknowns m_x, m_y, α_1 and α_2 need to be determined. The assumptions of compatibility of deformation and traction continuity over the discontinuity lines have

been used (see also Belytschko *et al.*, 1988). The addition of the localized mode to the standard shape functions that describe the motion of the body may not lead to additional nodal displacements. Therefore compatibility of deformation is assumed by means of

$$\int_{\Omega} \dot{\boldsymbol{\varepsilon}}\, \mathrm{d}\Omega = \int_{\Omega_1} \dot{\boldsymbol{\varepsilon}}_1\, \mathrm{d}\Omega_1 + \int_{\Omega_2} \dot{\boldsymbol{\varepsilon}}_2\, \mathrm{d}\Omega_2, \tag{29}$$

in which the total area of an element $\Omega = \Omega_1 + \Omega_2$ and $\dot{\boldsymbol{\varepsilon}} = \mathbf{B}\dot{\mathbf{a}}$ is the strain rate of the underlying element without additional modes. This condition coincides with a restriction that follows from the patch test, namely additional displacements due to extra non-conforming modes must vanish (Taylor *et al.*, 1986). Substituting eqns (8) and (9) into (29) gives

$$\int_{\Omega_1} -\alpha_1 \mathbf{q}\, \mathrm{d}\Omega_1 + \int_{\Omega_2} \alpha_2 \mathbf{q}\, \mathrm{d}\Omega_2 = 0. \tag{30}$$

Dependent on the type of element that is used the integrals from eqn (30) can be calculated and a relation

$$\alpha_1 = c\alpha_2 \quad \text{or} \quad \bar{\alpha}_1 = c\bar{\alpha}_2 \tag{31}$$

can be derived. For the three-noded element that is used in Section 6 we have $c = \Omega_2/\Omega_1$. Furthermore, we assume traction continuity in a direction perpendicular to the discontinuity. So, if we consider the local n, t-coordinate system we assume that

$$\begin{pmatrix} [\![\dot{t}^{\mathrm{m}}]\!] \\ [\![\dot{t}^{\mathrm{nt}}]\!] \end{pmatrix} = \mathbf{0}, \tag{32}$$

which equals

$$\mathbf{N}^{\mathrm{T}}\dot{\boldsymbol{\sigma}}_1 - \mathbf{N}^{\mathrm{T}}\dot{\boldsymbol{\sigma}}_2 = \mathbf{0}, \tag{33}$$

in which eqns (15) and (27) can be substituted which gives

$$\mathbf{N}^{\mathrm{T}}\mathbf{D}^{\mathrm{e}}\dot{\boldsymbol{\varepsilon}}_1 - \mathbf{N}^{\mathrm{T}}[\mathbf{D}^{\mathrm{e}} - \mathbf{D}^*]\dot{\boldsymbol{\varepsilon}}_2 = \mathbf{0}. \tag{34}$$

Now, the strain fields with the localized modes according to eqns (8) and (9) can be used to obtain

$$\mathbf{N}^{\mathrm{T}}\mathbf{D}^{\mathrm{e}}(\mathbf{B}\dot{\mathbf{a}} - \dot{\bar{\alpha}}_1\mathbf{q}) = \mathbf{N}^{\mathrm{T}}[\mathbf{D}^{\mathrm{e}} - \mathbf{D}^*](\mathbf{B}\dot{\mathbf{a}} + \dot{\bar{\alpha}}_2\mathbf{q}), \tag{35}$$

which can be rewritten in

$$\mathbf{N}^{\mathrm{T}}[(1+c)\mathbf{D}^{\mathrm{e}} - \mathbf{D}^*]\dot{\bar{\alpha}}_2\mathbf{q} = \mathbf{N}^{\mathrm{T}}\mathbf{D}^*\mathbf{B}\dot{\mathbf{a}}, \tag{36}$$

when $\bar{\alpha}_1 = c\bar{\alpha}_2$ is used. This results in a system of two equations with the unknowns $\bar{\alpha}_2$, m_x and m_y. Rewriting the left-hand side as

$$\mathbf{A}\mathbf{g} = \mathbf{N}^{\mathrm{T}}\mathbf{D}^*\mathbf{B}\dot{\mathbf{a}}, \tag{37}$$

with

$$g_x = \bar{\alpha}_2 m_x \tag{38}$$

$$g_y = \bar{\alpha}_2 m_y \tag{39}$$

and if we solve eqn (37) for g_x and g_y and combine this with the normality condition

$$m_x^2 + m_y^2 = 1, \tag{40}$$

it follows that

$$\bar{\alpha}_2 = \sqrt{g_x^2 + g_y^2}, \tag{41}$$

which means that with $m_x = g_x/\bar{\alpha}_2$, $m_y = g_y/\bar{\alpha}_2$ and $\bar{\alpha}_1 = c\bar{\alpha}_2$ the system is completely solved. The angle θ can be kept constant (fixed discontinuity model) or updated every step and iteration (rotating discontinuity model) but the vector **m** and the amplitudes $\bar{\alpha}_1$ and $\bar{\alpha}_2$ continuously change during computation. The vector **m** is uncoupled from vector **n** and therefore not necessarily aligned with **n**, which allows for mixed-mode effects.

4. MODE-II FAILURE

For the case of mode-II failure a plasticity concept is applied. Plastic deformation occurs in the discontinuity band and elastic deformation occurs outside of it. Again, for the elastic part Ω_1 we have

$$\dot{\boldsymbol{\varepsilon}}_1 = \dot{\boldsymbol{\varepsilon}}_1^e \tag{42}$$

and

$$\dot{\boldsymbol{\sigma}}_1 = \mathbf{D}^e \dot{\boldsymbol{\varepsilon}}_1. \tag{43}$$

For the plastic part of the element Ω_2 we decompose the total strain rate into elastic and plastic parts according to

$$\dot{\boldsymbol{\varepsilon}}_2 = \dot{\boldsymbol{\varepsilon}}_2^e + \dot{\boldsymbol{\varepsilon}}_2^p. \tag{44}$$

The stress–strain relation can be written as

$$\dot{\boldsymbol{\sigma}}_2 = \mathbf{D}^e(\dot{\boldsymbol{\varepsilon}}_2 - \dot{\boldsymbol{\varepsilon}}_2^p). \tag{45}$$

For associative plasticity the plastic strain rate vector is defined as

$$\dot{\boldsymbol{\varepsilon}}_2^p = \dot{\lambda}\bar{\mathbf{n}}, \tag{46}$$

in which $\dot{\lambda}$ is a non-negative scalar and $\bar{\mathbf{n}}$ a vector, representing the magnitude and the direction of the plastic flow, respectively. The vector $\bar{\mathbf{n}}$ is taken as the normal to the yield surface f according to

$$\bar{\mathbf{n}} = \frac{\partial f}{\partial \boldsymbol{\sigma}_2}. \tag{47}$$

The yield function f is a function of stress and the scalar-valued hardening/softening parameter κ. For plastic behavior we define

$$f(\boldsymbol{\sigma}_2, \kappa) = 0 \quad \text{and} \quad \dot{f}(\boldsymbol{\sigma}_2, \kappa) = 0 \tag{48}$$

with the second condition known as the consistency condition, which can be elaborated as

$$\bar{\mathbf{n}}^{\mathrm{T}} \dot{\boldsymbol{\sigma}}_2 + \frac{\partial f}{\partial \kappa} \dot{\kappa} = 0. \tag{49}$$

If we define the softening modulus h as

$$h = -\frac{1}{\dot{\lambda}} \frac{\partial f}{\partial \kappa} \dot{\kappa} \tag{50}$$

an explicit expression for the magnitude of the plastic flow can be derived by premultiplying eqn (45) by $\bar{\mathbf{n}}^{\mathrm{T}}$. Combination with eqns (46), (49) and (50) then yields

$$\dot{\lambda} = \frac{\bar{\mathbf{n}}^{\mathrm{T}} \mathbf{D}^{\mathrm{e}} \dot{\boldsymbol{\varepsilon}}_2}{h + \bar{\mathbf{n}}^{\mathrm{T}} \mathbf{D}^{\mathrm{e}} \bar{\mathbf{n}}}. \tag{51}$$

We can now obtain the relation between stress rate and strain rate by substitution of eqn (51) in eqn (45)

$$\dot{\boldsymbol{\sigma}}_2 = (\mathbf{D}^{\mathrm{e}} - \mathbf{D}^*) \dot{\boldsymbol{\varepsilon}}_2, \tag{52}$$

with

$$\mathbf{D}^* = \frac{\mathbf{D}^{\mathrm{e}} \bar{\mathbf{n}} \bar{\mathbf{n}}^{\mathrm{T}} \mathbf{D}^{\mathrm{e}}}{h + \bar{\mathbf{n}}^{\mathrm{T}} \mathbf{D}^{\mathrm{e}} \bar{\mathbf{n}}}. \tag{53}$$

The integration of this rate equation has been carried out with a standard implicit Euler backward return mapping scheme.

For the mode-II problem the inclination angle θ of the discontinuity plane with the x-axis is determined from a discontinuous bifurcation analysis. We make use of the acoustic tensor defined as

$$Q_{ijkl} = n_j (D^{\mathrm{e}}_{ijkl} - D^*_{ijkl}) n_l. \tag{54}$$

At the onset of localization at a local material point we have (see Hill, 1962; Rice, 1976)

$$\det(Q_{ijkl}) = 0. \tag{55}$$

After this point the determinant of the acoustic tensor becomes negative and the direction θ can be derived from (see Miehe and Schröder, 1994)

$$\frac{\mathrm{d}}{\mathrm{d}\theta}(\det(Q_{ijkl})) = 0. \tag{56}$$

If we fix the direction upon initiation of the shear band we again have a fixed discontinuity model. On the other hand, if we let θ rotate after initiation according to eqn (56) we have a rotating discontinuity model.

The jump coefficients $\bar{\alpha}_1$ and $\bar{\alpha}_2$ in eqns (8) and (9) are obtained from the compatibility condition and the assumption of stress continuity over the discontinuity line. So, eqn (29) holds which gives the $\bar{\alpha}_1 = c\bar{\alpha}_2$ relation and substituting $\mathbf{D}^*$ from eqn (53) into eqn (37) provides the explicit values for the jump coefficients $\bar{\alpha}_1$, $\bar{\alpha}_2$ and vector $\mathbf{m}$ according to the procedure described in Section 3.

5. FINITE ELEMENT DISCRETIZATION

To enforce equilibrium we assume at the end of the time or loading step

$$\mathbf{L}^{\mathrm{T}}\boldsymbol{\sigma}^{t-\Delta t} = \mathbf{0}. \tag{57}$$

The weak form of eqn (57) for an element with an elastic zone Ω_1 and a localized zone Ω_2 is as follows

$$\int_{\Omega_1} \delta\dot{\mathbf{u}}^{\mathrm{T}}[\mathbf{L}^{\mathrm{T}}\boldsymbol{\sigma}_1^{t-\Delta t}]\,\mathrm{d}\Omega_1 + \int_{\Omega_2} \delta\dot{\mathbf{u}}^{\mathrm{T}}[\mathbf{L}^{\mathrm{T}}\boldsymbol{\sigma}_2^{t+\Delta t}]\,\mathrm{d}\Omega_2 = 0, \tag{58}$$

or invoking the divergence theorem

$$\int_{\Omega_1} \delta\dot{\boldsymbol{\varepsilon}}_1^{\mathrm{T}}\boldsymbol{\sigma}_1^{t+\Delta t}\,\mathrm{d}\Omega_1 + \int_{\Omega_2} \delta\dot{\boldsymbol{\varepsilon}}_2^{\mathrm{T}}\dot{\boldsymbol{\sigma}}_2^{t-\Delta t}\,\mathrm{d}\Omega_2 - \int_S \delta\dot{\mathbf{u}}^{\mathrm{T}}\mathbf{p}^{t+\Delta t}\,\mathrm{d}S = 0, \tag{59}$$

in which $\mathbf{p}$ are the tractions at boundary S. For an incremental–iterative procedure the stress at time $t+\Delta t$ in both parts is decomposed into the stress at time t and the stress increment

$$\boldsymbol{\sigma}_{1,2}^{t+\Delta t} = \boldsymbol{\sigma}_{1,2}^{t} + \Delta\boldsymbol{\sigma}_{1,2}, \tag{60}$$

which can be substituted into eqn (59)

$$\int_{\Omega_1} \delta\dot{\boldsymbol{\varepsilon}}_1^{\mathrm{T}}\Delta\boldsymbol{\sigma}_1\,\mathrm{d}\Omega_1 + \int_{\Omega_2} \delta\dot{\boldsymbol{\varepsilon}}_2^{\mathrm{T}}\Delta\boldsymbol{\sigma}_2\,\mathrm{d}\Omega_2 = \int_S \delta\dot{\mathbf{u}}^{\mathrm{T}}\mathbf{p}^{t+\Delta t}\,\mathrm{d}S - \int_{\Omega_1} \delta\dot{\boldsymbol{\varepsilon}}_1^{\mathrm{T}}\sigma_1^{t}\,\mathrm{d}\Omega_1 - \int_{\Omega_2} \delta\dot{\boldsymbol{\varepsilon}}_2^{\mathrm{T}}\boldsymbol{\sigma}_2^{t}\,\mathrm{d}\Omega_2 \tag{61}$$

The constitutive equations in linearized format can be used in eqn (61) to obtain

$$\int_{\Omega_1} \delta\dot{\boldsymbol{\varepsilon}}_1^{\mathrm{T}}\mathbf{D}^{\mathrm{c}}\Delta\boldsymbol{\varepsilon}_1\,\mathrm{d}\Omega_1 + \int_{\Omega_2} \delta\dot{\boldsymbol{\varepsilon}}_2^{\mathrm{T}}\mathbf{D}^{\mathrm{c}}\Delta\boldsymbol{\varepsilon}_2\,\mathrm{d}\Omega_2 = \int_S \delta\dot{\mathbf{u}}^{\mathrm{T}}\mathbf{p}^{t+\Delta t}\,\mathrm{d}S - \int_{\Omega_1} \delta\dot{\boldsymbol{\varepsilon}}_1^{\mathrm{T}}\boldsymbol{\sigma}_1^{t}\,\mathrm{d}\Omega_1 - \int_{\Omega_2} \delta\dot{\boldsymbol{\varepsilon}}_2^{\mathrm{T}}\boldsymbol{\sigma}_2^{t}\,\mathrm{d}\Omega_2, \tag{62}$$

in which $\mathbf{D}^{\mathrm{c}} = \mathbf{D}^{\mathrm{c}} - \mathbf{D}^{*}$ with $\mathbf{D}^{*}$ for mode-I failure given in eqn (28) and for mode-II failure given in eqn (53). Now for $\boldsymbol{\varepsilon}_1$ and $\boldsymbol{\varepsilon}_2$ the enhanced strain fields according to eqns (10) and (11) can be substituted. Together with eqn (7) and the assumption that the equation must hold for any admissible field $\delta\dot{\mathbf{a}}$ transforms eqn (62) in

$$\mathbf{K}\Delta\mathbf{a} = \mathbf{f}_{\mathrm{e}} - \mathbf{f}_{\mathrm{i}}, \tag{63}$$

in which

$$\mathbf{K} = \int_{\Omega_1} \bar{\mathbf{B}}_1^{\mathrm{T}}\mathbf{D}^{\mathrm{c}}\bar{\mathbf{B}}_1\,\mathrm{d}\Omega_1 + \int_{\Omega_2} \bar{\mathbf{B}}_2^{\mathrm{T}}\mathbf{D}^{\mathrm{c}}\bar{\mathbf{B}}_2\,\mathrm{d}\Omega_2, \tag{64}$$

$$\mathbf{f}_{\mathrm{e}} = \int_S \mathbf{H}^{\mathrm{T}}\mathbf{p}^{t+\Delta t}\,\mathrm{d}S, \tag{65}$$

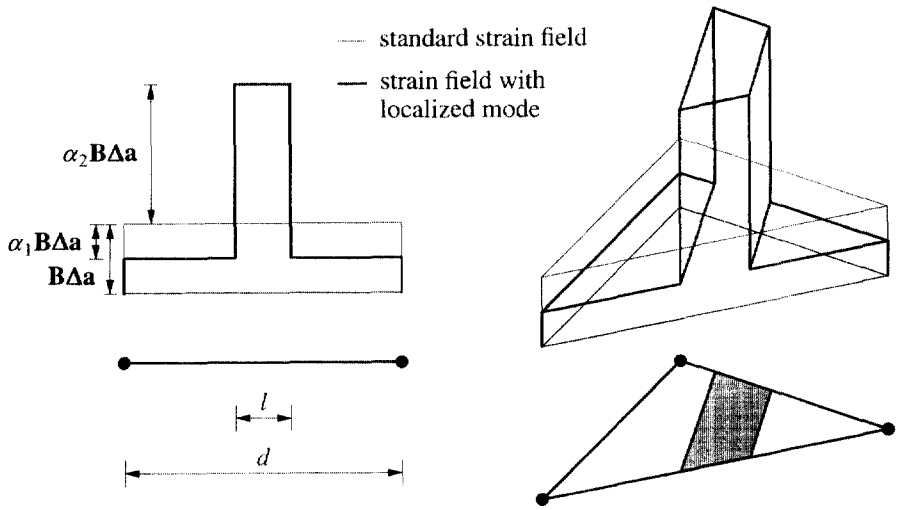

Fig. 2. Linear elements with additional discontinuous shape functions. Left: truss element and right: triangular element.

$$\mathbf{f}_i = \int_{\Omega_1} \bar{\mathbf{B}}_1^{\mathrm{T}} \sigma_1' \, \mathrm{d}\Omega_1 + \int_{\Omega_2} \bar{\mathbf{B}}_2^{\mathrm{T}} \boldsymbol{\sigma}_2' \, \mathrm{d}\Omega_2, \tag{66}$$

A two-noded truss element and a three-noded triangular element have been used in this study (see Fig. 2). Both elements have one integration point in which we define a dual set of stresses $\boldsymbol{\sigma}_1$ and $\boldsymbol{\sigma}_2$ and strains $\boldsymbol{\varepsilon}_1$ and $\boldsymbol{\varepsilon}_2$ corresponding to the elastic part and the localized part. To carry out a proper integration of the eqns (64)–(66) the areas Ω_1 and Ω_2 have to be determined. The centre of the localization band is assumed to go through the integration point and its width is set by the length scale parameter l. In the two-dimensional element also a length of the discontinuity line has to be specified. Belytschko *et al.* (1988) proposed

$$a = \sqrt{\Omega}, \tag{67}$$

with Ω the total area of the finite element. We can also calculate a correctly, i.e. dependent on the angle under which the localized mode is superimposed. The effect of the choice for a will be discussed in the next section.

6. EXAMPLES

First, the pure mode-I problem will be discussed. In this case the normal to the failure plane $\mathbf{n}$ is aligned with vector $\mathbf{m}$, i.e. $\mathbf{n}^{\mathrm{T}} = \mathbf{m}^{\mathrm{T}} = (1, 0)^{\mathrm{T}}$. Hence, after the addition of the localized mode the incremental strains outside and inside the localization zone according to eqns (8) and (9) reduce to

$$\Delta\varepsilon_1 = (1 - \alpha_1)\mathbf{B}\Delta\mathbf{a} \tag{68}$$

and

$$\Delta\varepsilon_2 = (1 + \alpha_2)\mathbf{B}\Delta\mathbf{a}, \tag{69}$$

with $\mathbf{B} = (1/d)[-1, 1]$ for a two-noded truss element and with α_1 and α_2 the amplitudes of the localized mode as given in Fig. 2. The length of the truss element is d and l is the localization band width as explained in Section 2. The amplitudes α_1 and α_2 can be determined from compatibility and traction continuity. For the two-noded truss element condition (29) results in

$$d\mathbf{B}\Delta\mathbf{a} = (d-l)\Delta\varepsilon_1 + l\Delta\varepsilon_2, \tag{70}$$

which after use of eqns (68) and (69) leads to

$$\alpha_1 = \left(\frac{l}{d-l}\right)\alpha_2. \tag{71}$$

The assumption of traction continuity [eqn (33)] in 1-D format yields

$$\Delta\sigma_1 = \Delta\sigma_2. \tag{72}$$

The constitutive equations for the elastic and localized part are given in eqns (15) and (27), respectively. If we only consider the normal component and substitute these expressions into eqn (72) we obtain

$$E\Delta\varepsilon_1 = \left(E - \frac{E^2}{E+h}\right)\Delta\varepsilon_2, \tag{73}$$

with E the Young's modulus. The softening modulus is taken here as a constant equal to $h = -f_t/\varepsilon_u$, with f_t the tensile strength and ε_u the ultimate strain. Combination of eqn (73) with (68), (69) and (71) gives an explicit expression for the amplitudes

$$\alpha_1 = \frac{(l/(d-l))E}{h+(E+h)(l/(d-l))} \tag{74}$$

and

$$\alpha_2 = \frac{E}{h+(E+h)(l/(d-l))}. \tag{75}$$

So, α_1 and α_2 are functions of h. If we have nonlinear softening the mode amplitudes change during local iterations for an accurate stress update.

A tension bar modelled with truss elements (Fig. 3) is analyzed with and without the inclusion of localized modes. Two different meshes have been used with 20 and 40 truss

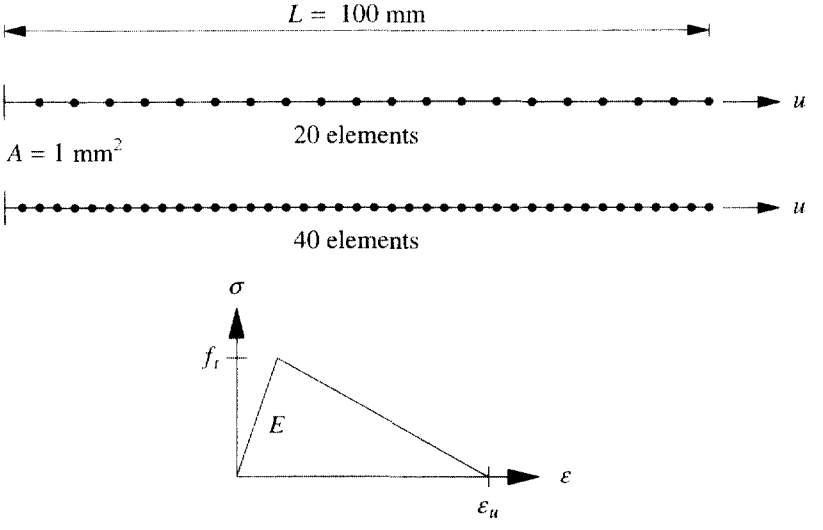

Fig. 3. One-dimensional tension bar with two-noded truss elements.

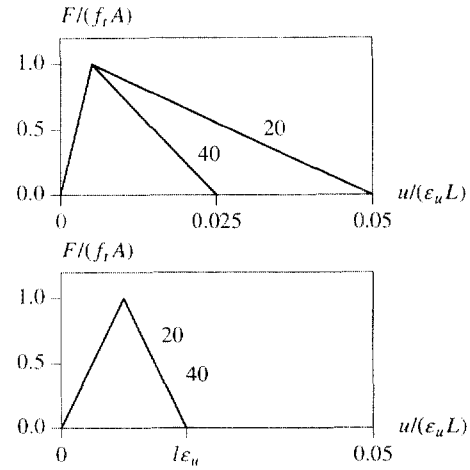

Fig. 4. Load–displacement curves. Top: standard element. Bottom: discontinuity elements.

elements, respectively. The length of the bar $L = 100$ mm and the cross-section $A = 1$ mm^2. The material parameter set is as follows: the Young's modulus $E = 10.000$ N/mm^2, the tensile strength $f_t = 1$ N/mm^2, the ultimate strain $\varepsilon_u = 0.01$ and the localization band width $l = 2$ mm. One element at the left boundary is given a small material imperfection. The effect of the localized mode with a fixed width l on the load-displacement curve ($F-u$) is clear. With standard elements without the additional mode (Fig. 4—top) the results are mesh dependent. More elements produce a more brittle response. Use of the weak discontinuity elements with the same value for l in the analyses with the different meshes solves this problem (Fig. 4—bottom).

Secondly, we will analyze localization in pure shear. For the mode-II case the normal to the failure plane $\mathbf{n}$ is perpendicular to vector $\mathbf{m}$, i.e. $\mathbf{n}^T = (1, 0)^T$ and $\mathbf{m}^T = (0, 1)^T$. With eqns (10) and (11) it is clear that the localized mode is only added to the shear strain parallel to the shear band and we obtain

$$\Delta\gamma_1 = (1 - \alpha_1)\mathbf{B}\Delta\mathbf{a} \tag{76}$$

and

$$\Delta\gamma_2 = (1 + \alpha_2)\mathbf{B}\Delta\mathbf{a}, \tag{77}$$

in which $\mathbf{a}$ now contains the vertical displacements. The compatibility condition for the pure mode-II case results in the same dependence between the mode amplitudes as in the mode-I case

$$\alpha_1 = \left(\frac{l}{d-l}\right)\alpha_2, \tag{78}$$

in which l now is the width of the shear band. Traction continuity over the shear band reads

$$\Delta\tau_1 = \Delta\tau_2. \tag{79}$$

If we use the constitutive equations for the elastic part [eqn (43)] and for the localized part [eqn (52)] we obtain

$$G\Delta\gamma_1 = \frac{hE}{2h+3E}\Delta\gamma_2, \tag{80}$$

in which $G = E/2$ the shear modulus and h the softening modulus as generally defined in eqn (50). To specify h we assume a Von Mises type yield function according to

$$f(\tau_2, \kappa) = \sqrt{3}\tau_2 - \bar{\sigma}(\kappa), \tag{81}$$

with $\bar{\sigma}$ the yield stress as a function of the equivalent plastic strain κ and assume a strain-softening hypothesis

$$\dot{\kappa} = \frac{\dot{\gamma}_2}{\sqrt{3}}. \tag{82}$$

Then expression (50) for the softening modulus reduces to

$$h = \frac{\mathrm{d}\bar{\sigma}}{\mathrm{d}\kappa}. \tag{83}$$

If we take linear softening we have $h = -\bar{\sigma}_0/\kappa_u$, in which $\bar{\sigma}_0$ is the initial yield stress and κ_u is the ultimate equivalent plastic strain. Again, combination of eqn (80) with (76), (77) and (78) gives the explicit expressions for the amplitudes

$$\alpha_1 = \frac{3El}{3El+2hd} \tag{84}$$

and

$$\alpha_2 = \frac{3E(d-l)}{3El+2hd}. \tag{85}$$

For the mode-II problem we analyzed a shear layer (Fig. 5) that has been modelled with the three-noded triangular element (see Fig. 2). All displacements in horizontal direction are zero to avoid bending effects. The shear layer has the same dimensions as the tension bar discussed above. The material parameter set is as follows: the Young's modulus $E = 20.000$ N/mm^2, the initial yield stress $\bar{\sigma}_0 = \sqrt{3}$ N/mm^2, the ultimate equivalent plastic strain

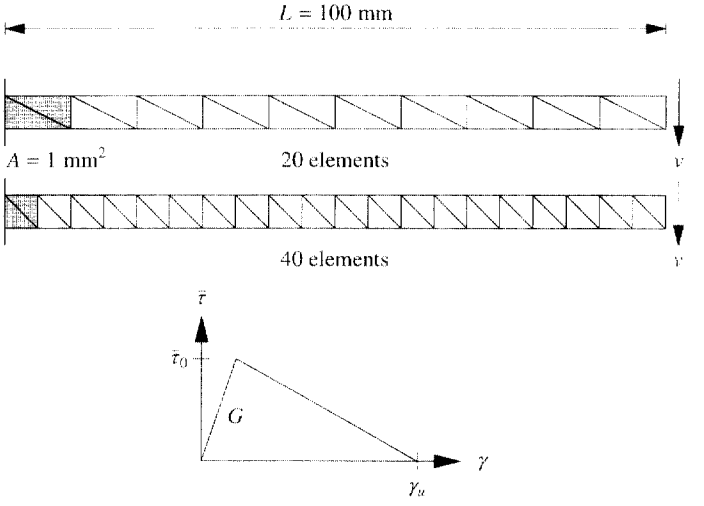

Fig. 5. Shear layer with three-noded triangular elements.

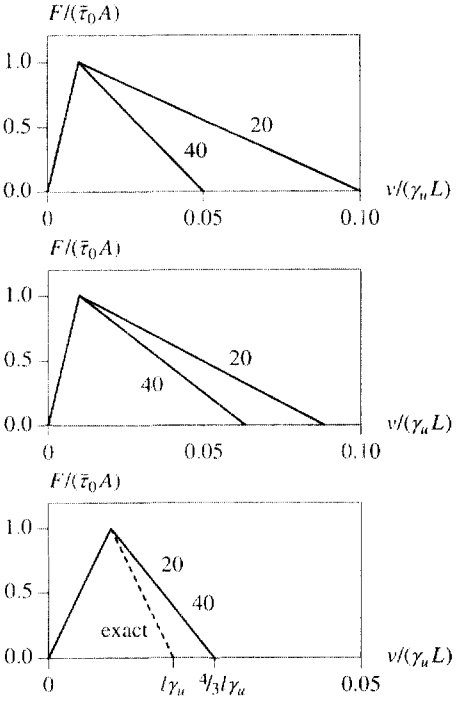

Fig. 6. Load-displacement curves. Top: standard element. Centre: discontinuity element with $a = \sqrt{\Omega}$. Bottom: discontinuity element with a is "exact".

$\kappa_u = 0.01/\sqrt{3}$ and the shear band width $l = 2$ mm. These parameters result in a shear modulus $G = 10.000$ N/mm^2, an initial shear yield stress $\bar{\tau}_0 = 1$ N/mm^2 and an ultimate shear strain $\gamma_u = 0.01$. This makes the problem equivalent to the tension problem. In both meshes (20 and 40 elements) two elements have been given a small material imperfection. With the standard constant strain triangle we obtain the same mesh-dependent results as for the standard truss elements for mode-I localization (Fig. 6—top). For the discontinuity elements the results heavily depend on the definition of the shear band length a. If we take $a = \sqrt{\Omega}$ [eqn (67)] the load–deformation curve from Fig. 6—centre is obtained. For this mode-II problem the mesh dependence is still there because mesh refinement leads to a smaller area Ω of an element and therefore to a decrease of a and a decrease of the strain energy consumption in this configuration. This problem becomes more significant with a high aspect ratio of the finite element. If we calculate a correctly, i.e. dependent on the angle under which the localized mode is superimposed, the results can be made mesh objective (see Fig. 6—bottom). Remarkable then is that the ultimate deformation is larger than the analytical value $l\gamma_u$ (see dashed line in Fig. 6—bottom). This is due to the overlap in shear band length between the two shear bands in the two imperfect elements. The shear band in each of the two elements goes through the integration point of the triangle which results in a length of 2/3 mm per element and 4/3 mm in total. For this reason we slightly overestimate the ultimate deformation in a set-up as shown here.

A two-dimensional analysis of shear banding in a biaxial test has been carried out. The influence of mesh size and mesh orientation has been analyzed. The sample is fixed at the bottom in vertical direction and compressed at the top with a constant velocity. The length of the sample is 12 mm and the width is 6 mm. The material parameter set is as follows: the Young's modulus $E = 20.000$ N/mm^2, Poisson's ratio $\nu = 0.3$, the initial yield stress $\bar{\sigma}_0 = 20$ N/mm^2, the ultimate equivalent plastic strain $\kappa_u = 0.05$ and the shear band width $l = 0.2$ mm. Again Von Mises plasticity with linear strain softening has been used with plane strain elements. The fixed discontinuity concept as described in Section 3 has been applied and the shear band length per element a is calculated exactly. One element at the left side of the sample is given a small material imperfection. First two structured meshes with 144 and 576 elements, respectively, have been analyzed. The deformed models and

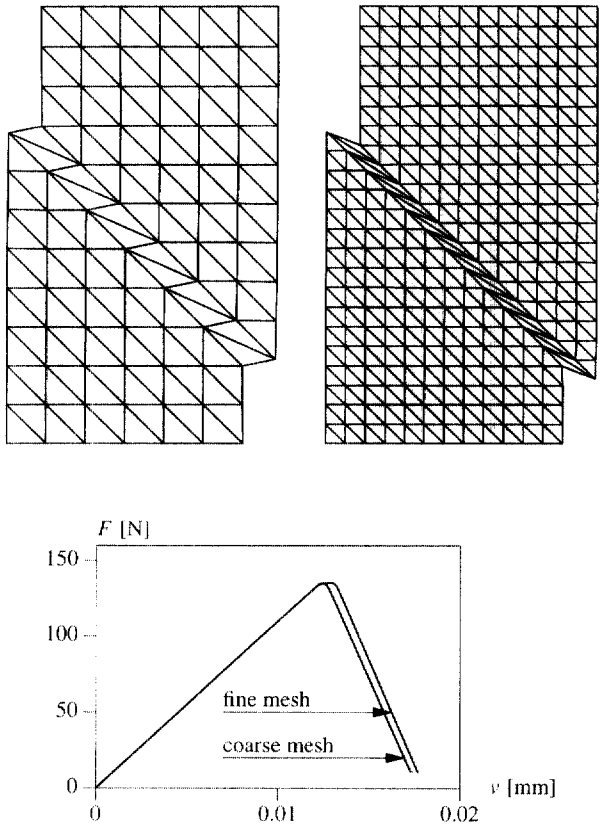

Fig. 7. Top: deformed model structured meshes. Bottom: load–displacement curve.

the load–displacement curve show mesh-size independence (see Fig. 7). The slope of the descending branch is determined by the softening modulus and the length scale parameter.

Next two unstructured meshes have been used to investigate the influence of mesh orientation. The fully unstructured mesh (Fig. 8—left) gives different results with respect

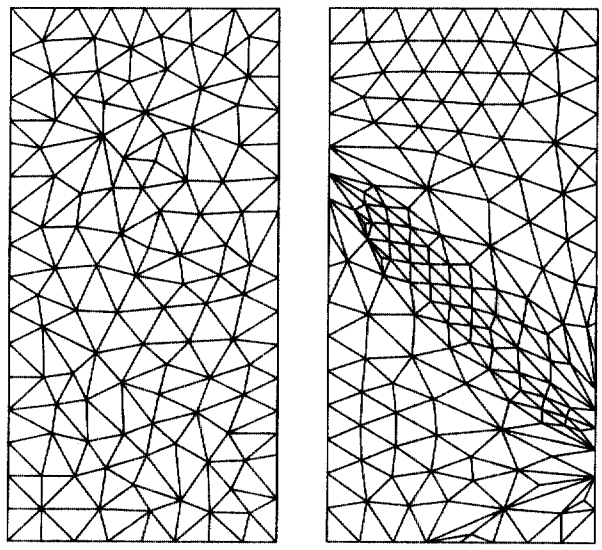

Fig. 8. Left: unstructured mesh. Right: unstructured "aligned" mesh.

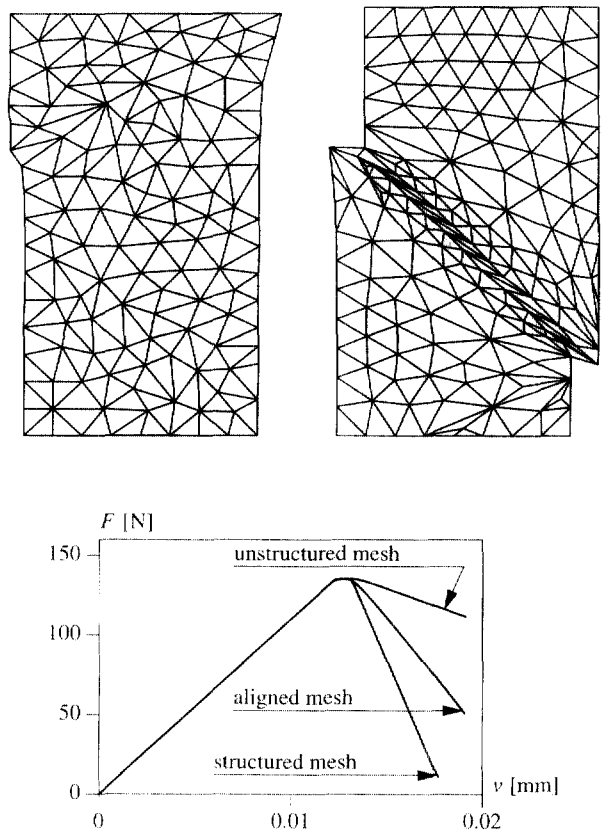

Fig. 9. Top: deformed model unstructured meshes. Bottom: load–displacement curve.

to the structured meshes. From Fig. 9 it is observed that a different failure mode is triggered by this finite element configuration. The load–displacement diagram also shows locking behavior of the solution. This is a well known property of the underlying constant strain triangle. This behavior can be improved by the addition of extra continuous shape functions (e.g. bubble functions, see Armero and Garikipati, 1995). A second unstructured mesh has been used for which a realignment procedure has been used (Fig. 8—right). The mesh is aligned with the shear band on the basis of the acoustic tensor (Sluys *et al.*, 1998). Now, a proper shear band can be calculated, however, the load–displacement diagram shows a slightly more ductile response than the structured mesh.

7. COMPARISON WITH STANDARD MODELS

The similarities and differences between the model presented here and the standard models for the description of failure will be discussed. For instance, for mode-I fracture the crack band model (Pietruszczak and Mróz, 1981; Bažant and Oh, 1983; Willam, 1984; Rots, 1988) is widely used. In this model the crack is smeared over the finite element and the softening modulus is made a function of the finite element size. It can be shown that the weak discontinuity model for mode-I failure as discussed in Section 3 provides exactly the same set of discretized equations as for the crack band model in the one-dimensional case under pure mode-I loading and with the length scale in the discontinuity model taken equal to the element size (see Berends, 1996). In general the formulations are different and a first advantage of the discontinuity model is that the length scale parameter l acts as a material parameter and is not dependent on the mesh. Due to this and the proper calculation of the crack length a the area per element that goes into softening is calculated in a proper way. On the other hand, for the crack band model this is still a undefined issue. Actually, the so-called crack band width is taken independent of the direction of crack propagation

and is also independent of the aspect ratio of a finite element. However, this may cause a considerable under- or overestimation of the energy consumed in the crack and a mesh dependence. The discontinuity model can be improved by connecting the crack between elements. An overlap of cracks or shear bands as shown in the previous section is then excluded. A second advantage of the weak discontinuity model presented here is that mesh sensitivity of the shear component of the crack strain is solved. Namely, in the crack band model the shear reduction factor β is a constant and not a function of the element size. As a consequence, the use of a finer mesh leads to a smaller cracked area in which the shear stiffness is reduced and to mesh dependence. On the other hand, in the discontinuity model the area in which the shear stiffness is reduced is set by l and is not a function of the element size. A mesh-dependent effect is therefore excluded.

8. CONCLUSIONS

The use of continuum models for the description of failure leads to mesh-objective results when a length scale parameter is introduced in the formulation. A disadvantage of such a continuum formulation is that very fine meshes are needed to obtain an accurate strain profile inside the localization zone. For this reason, the discrete approach in which the localization zone in thickness direction is captured in one element seems to be more appealing for large scale computations. In this paper a model with discontinuous functions of the displacement gradient is used. An additional localized mode is added to the standard shape functions of the finite element. A length scale parameter is introduced which is a material parameter and can be related to the size of the fracture process zone or the width of the shear band. The amplitudes of the localized mode are obtained from the traction continuity condition that must be satisfied over the discontinuity line and the assumption of compatibility of deformation. The model can be combined with different sets of constitutive equations. Here we elaborated the model for a fracture model and a plasticity model. Simple mode-I and mode-II problems have been analyzed to reveal the performance of the model with respect to mesh-size and mesh-orientation sensitivity. From the two-dimensional analysis with an unstructured mesh it can be seen that the problem of mesh alignment is not solved with this weak discontinuity model. In this case the concept should be combined with a mesh-realignment strategy. Furthermore, a comparison with standard continuum models for fracture shows the similarities for a specific one-dimensional case and the differences with respect to the role of the length scale parameter and the behavior of the models under mode-II loading conditions.

Acknowledgements—Financial support of the Royal Netherlands Academy of Arts and Sciences to the first author is gratefully acknowledged.

REFERENCES

Aifantis, E. C. (1984) On the microstructural origin of certain of certain models. *J. Engng Mater. Technol.* **106,** 326–334.

Armero, F. and Garikipati, K. (1995) Recent advances in the analysis and numerical simulation of strain localization in inelastic solids. *Computational Plasticity. Fundamentals and Applications*, ed. D. R. J. Owen and E. Oñate, pp. 547–561. Pineridge Press, Swansea.

Bažant, Z. P. and Oh, B. (1983) Crack band theory for fracture of concrete. *Mat. and Struct.* **16,** 155–177.

Belytschko, T., Fish, J. and Engelman, B. E. (1988) A finite element with embedded localization zones. *Comp. Meth. Applied Mech. Engng* **70,** 59–89.

Berends, A. H. (1996) Cracks in brittle materials. Graduation Report, Delft University of Technology, Delft.

de Borst, R., Sluys, L. J., Mühlhaus, H.-B. and Pamin, J. (1993) Fundamental issues in finite element analyses of localization of deformation. *Engng Comput.* **10,** 99–121.

Hill, R. (1962) Acceleration waves in solids. *Journal of the Mechanics and Physics of Solids* **10,** 1–16.

Klisinski, M., Runesson, K. and Sture, S. (1991) Finite element with inner softening band. *ASCE J. Eng. Mech.* **17,** 575–587.

Larsson, R. (1990) Numerical simulation of plastic localization. Dissertation, Chalmers University of Technology, Göteborg.

Larsson, R. and Runesson, K. (1996) Element-embedded localization band based on regularized displacement discontinuity. *ASCE J. Eng. Mech.* **122,** 402–411.

Larsson, R., Runesson, K. and Akesson, M. (1995) Embedded localization based on regularized strong discontinuity, *Computational Plasticity, Fundamentals and Applications*, ed. D. R. J. Owen and E. Oñate, pp. 599–610. Pineridge Press, Swansea.

Lasry, D. and Belytschko, T. (1988) Localization limiters in transient problems. *International Journal of Solids and Structures* **24,** 581–597.

Lofti, H. R. and Shing, P. B. (1995) Embedded representation of fracture in concrete with mixed finite elements. *International Journal of Numerical Methods in Engineering* **38,** 1307–1325.

Miehe, C. and Schröder, J. (1994) Post-critical discontinuous localization analysis of small-strain softening elastoplastic solids. *Archive of Applied Mechanics* **64,** 267.

Mühlhaus, H.-B. and Aifantis, E. C. A variational principle for gradient plasticity. *International Journal of Solids and Structures* **28,** 845–858.

Needleman, A. (1988) Material rate dependence and mesh sensitivity on localization problems. *Comp. Meth. Appl. Mech. Engng* **67,** 69–86.

Ortiz, M., Leroy, Y. and Needleman, A. (1987) A finite element method for localized failure analysis. *Comp. Meth. Appl. Mech. Engng* **61,** 189–214.

Pietruszczak, S. and Mróz, Z. (1981) Finite element analysis of deformation of strain softening materials. *International Journal of Numerical Methods in Engineering* **17,** 327–334.

Pijaudier-Cabot, G. and Bažant, Z. P. (1987) Nonlocal damage theory. *ASCE J. Eng. Mech.* **113,** 1512–1533.

Rice, J. R. (1976) The localization of plastic deformation. *Theoretical and Applied Mechanics*, ed. W. T. Koiter, pp. 207–220. North Holland Publishing Company, Amsterdam.

Rots, J. G. (1988) Computational modeling of concrete fracture. Dissertation, Delft University of Technology, Delft.

Simo, J. C. and Oliver, J. (1994) A new approach to the analysis and simulation of strong discontinuities. *Fracture and Damage in Quasibrittle Structures*, ed. Z. P. Bažant *et al.*, pp. 25–39. E&FN Spon.

Simo, J. C., Oliver, J. and Armero, F. (1993) An analysis of strong discontinuities induced by softening solutions in rate-independent solids. *J. Comput. Mech.* **12,** 277–296.

Sluys, L. J. (1992) Wave propagation, localisation and dispersion in softening solids. Dissertation. Delft University of Technology, Delft.

Sluys, L. J., Bićanić, N. and Pearce, C. J. (1998) Mesh-realignment studies in mode-I and mode-II localization problems, in preparation.

Sluys, L. J., Mühlhaus, H.-B. and de Borst, R. (1992) Wave propagation, localization and dispersion in a gradient-dependent medium. *International Journal of Solids and Structures* **30,** 1153–1171.

Taylor, R. L., Simo, J. C., Zienkiewicz, O. Z. and Chan, A. C. H. (1986) The patch test—a condition for assessing FEM convergence. *International Journal of Numerical Methods in Engineering* **22,** 39–62.

Willam, K. (1984) Experimental and computational aspects of concrete fracture. In *Proc. Int. Conf. on Comp. Aided Analysis and Design of Concrete Structures*, ed. F. Damjanić *et al.*), pp. 33–70. Pineridge Press, Swansea.